



1 **The response of precipitation characteristics to global warming from global**
2 **and regional climate projections**

3 *Filippo Giorgi, Francesca Raffaele, Erika Coppola*

4 *1 Earth System Physics Section, The Abdus Salam International Centre for Theoretical*
5 *Physics, I-34151 Trieste, Italy*

6

7 Corresponding author: Filippo Giorgi, Earth System Physics Section, The Abdus Salam
8 International Centre for Theoretical Physics, Trieste, I-34151, Italy. Email: giorgi@ictp.it;
9 phone: +39 0402240425.

10

11 Submitted to: Earth System Dynamics

12

13



14

Abstract

15 We revisit the issue of the response of the precipitation characteristics to global warming
16 based on analyses of global and regional climate model projections for the 21st century. The
17 prevailing response we identify can be summarized as follows: increase in the intensity of
18 precipitation events and extremes, with the occurrence of events of "unprecedented"
19 magnitude, i.e. magnitude not found in present day climate; decrease in the number of light
20 precipitation events and in wet spell lengths; increase in the number of dry days and dry spell
21 lengths. This response, which is mostly consistent across the models we analyzed, is tied to the
22 difference between precipitation intensity responding to increases in local humidity
23 conditions, especially for heavy and extreme events, and mean precipitation responding to
24 slower increases in global evaporation. These changes in hydroclimatic characteristics have
25 multiple and important impacts on the Earth's hydrologic cycle and on a variety of sectors,
26 and as examples we investigate effects on the potential stress due to increases in dry and wet
27 extremes, changes in precipitation interannual variability and changes in potential
28 predictability of precipitation events. We also stress how the understanding of the
29 hydroclimatic response to global warming can shed important insights into the fundamental
30 behavior of precipitation processes, most noticeably tropical convection.

31 **Keywords:** Precipitation, climate change, hydrologic cycle, extremes

32

33 1. Introduction

34 One of the greatest concerns regarding the effects of climate change on human
35 societies and natural ecosystems is the response of the Earth's hydrologic cycle to global
36 warming. In fact, by affecting the surface energy budget, greenhouse gas (GHG) induced
37 warming, along with related feedback processes (e.g. the water vapor, ice albedo and cloud



38 feedbacks), can profoundly affect the Earth's water cycle (e.g. Trenberth et al. 2003; Held and
39 Soden 2006; Trenberth 2011; IPCC 2012).

40 The main engine for the Earth's hydrologic cycle is the radiation from the Sun, which
41 heats the surface and causes evaporation from the oceans and land. Total surface evaporation
42 has been estimated at $486 \cdot 10^3 \text{ km}^3/\text{year}$ of water, of which $413 \cdot 10^3 \text{ km}^3/\text{year}$, or $\sim 85\%$, is
43 from the oceans and the rest from land areas (Trenberth et al. 2007). Once in the atmosphere,
44 water vapor is transported by the winds until it eventually condenses and forms clouds and
45 precipitation. The typical atmospheric lifetime of water vapor is of several days, and therefore
46 at climate time scales there is essentially an equilibrium between global surface evaporation
47 and precipitation. Total mean precipitation as been estimated at $373 \cdot 10^3 \text{ km}^3/\text{year}$ of water
48 over oceans and $113 \cdot 10^3 \text{ km}^3/\text{year}$ over land (adding up to the same global value as
49 evaporation, Trenberth et al. 2007). Water precipitating over land can then either re-evaporate
50 or flow into the oceans through surface runoff or sub-surface flow.

51 Given this picture of the hydrologic cycle, however, it is important to stress that,
52 although evaporation and precipitation globally balance out, their underlying processes are
53 very different. Evaporation is a continuous and slow process (globally about $\sim 2.8 \text{ mm/day}$,
54 Trenberth et al. 2007), while precipitation is a highly intermittent, fast and localized
55 phenomenon, with precipitation events drawing moisture only from an area of about 3-5 times
56 the size of the event itself (Trenberth et al. 2003). In addition, on average, only about 25% of
57 days are rainy days (where throughout this paper a rainy day is considered has having a
58 precipitation amount of at least 1 mm/day , so that drizzle days are removed), but since it does
59 not rain throughout the entire day, the actual fraction of time it rains has been estimated at 5-
60 10% (Trenberth et al. 2003). In other words, most of the time it does not actually rain.



61 This has important implications for the assessment of hydroclimatic responses to
62 global warming, because it may not be very meaningful, and certainly not sufficient, to analyze
63 mean precipitation fields, but it is necessary to also investigate higher order statistics. For
64 example, the same mean of, say, 1 mm/day could derive from 10 consecutive 1 mm/day
65 events, a single 10 mm/day event with 9 dry days, or two 5 mm/day events separated by a dry
66 period. Each of these cases would have a very different impact on societal sectors or
67 ecosystem dynamics.

68 This consideration also implies that the impact of global warming on the Earth's
69 hydroclimate might actually manifest itself not only as a change in mean precipitation but,
70 perhaps more markedly, as variations in the characteristics and regimes of precipitation
71 events. This notion has been increasingly recognized since the pioneering works of Trenberth
72 (1999) and Trenberth et al. (2003), with many studies looking in particular at changes in the
73 frequency and intensity of extreme precipitation events (e.g. Easterling et al. 2000;
74 Christensen and Christensen 2003; Tebaldi et al. 2006; Allan and Soden 2008; Giorgi et al.
75 2011; IPCC 2012; Sillmann et al. 2013; Giorgi et al. 2014a,b).

76 In this paper we revisit some of the concepts related to the issue of the impacts of
77 global warming on the characteristics of the Earth's hydroclimate, stressing however that it is
78 not our purpose to provide a review of the extensive literature on this topic. Rather, we want
79 to illustrate some of the points made above through relevant examples obtained from new and
80 past analyses of global and regional climate model projections.

81 More specifically, we will draw from global climate model (GCM) projections carried
82 out as part of the CMIP5 program (Taylor et al. 2012) and regional climate model (RCM)
83 projections from the COordinated Regional climate Downscaling EXperiment (CORDEX,
84 Giorgi et al. 2009; Jones et al. 2011, Gutowski et al. 2016), which downscale CMIP5 GCM



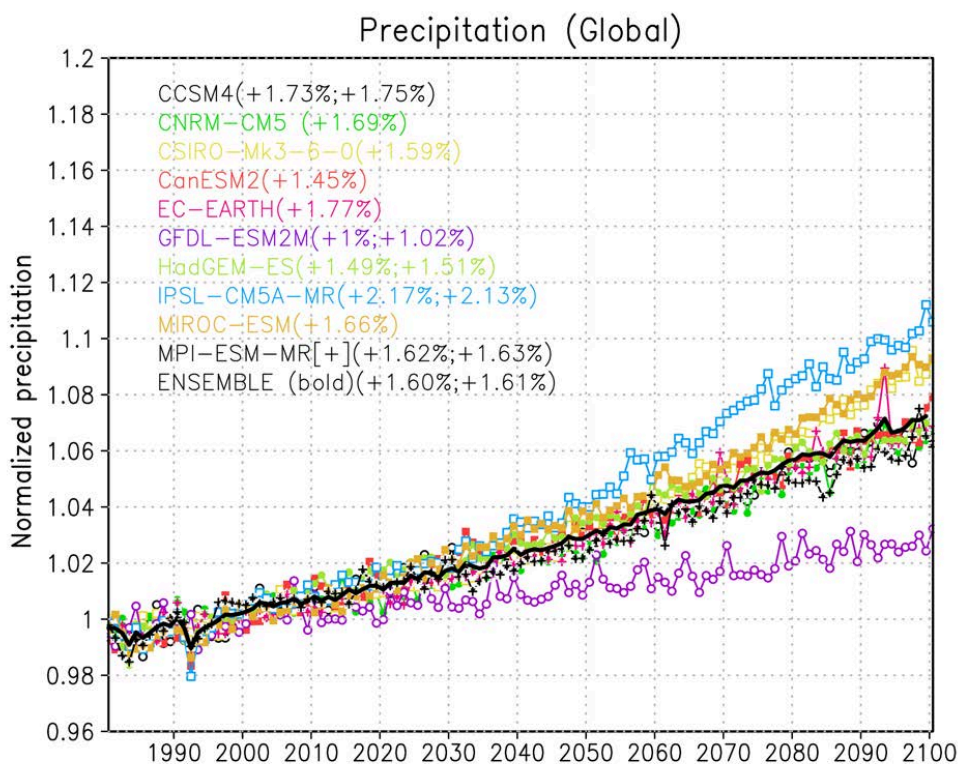
85 data. In this regard, we focus on the high end RCP8.5 scenario, in which the ensemble mean
86 global temperature increase by 2100 is about 4°C (+/- 1°C) compared to late 20th century
87 temperatures (IPCC 2013), stressing that results for lower GHG scenarios are qualitatively
88 similar to those found here but of smaller magnitude (not shown for brevity).

89 In the next sections we first summarize the changes in mean precipitation fields in our
90 ensemble of model projections, and then explore the response of different precipitation
91 characteristics, trying specifically to identify robust responses. After having identified the
92 dominant hydroclimatic responses, we discuss examples of their impact on different quantities
93 of relevance for socio-economic impacts, and specifically the potential stress associated with
94 changes in dry and wet extreme events, precipitation interannual variability and predictability
95 of precipitation events.

96 **2. The hydroclimatic response to global warming**

97 ***2.1 Mean precipitation changes***

98 In general, as a result of the warming of the oceans and land, global surface
99 evaporation increases with increasing GHG forcing. This increase mostly lies in the range of
100 1-2 % per degree of surface global warming (%/DGW; Trenberth et al. 2007). As a
101 consequence, global mean precipitation also tends to increase roughly by the same amount.
102 This has been found in most GCM projections, as illustrated in the examples of Figure 1.



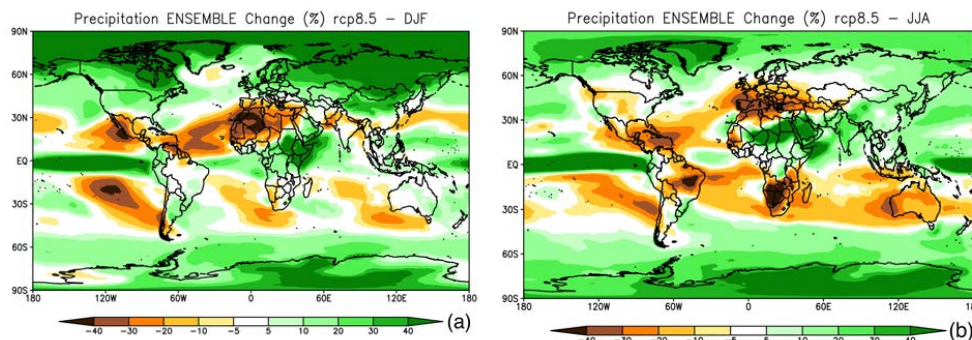
103
104 **Figure 1.** Normalized mean global precipitation from 1981 to 2100 in the 10 CMIP5 GCMs simulation for the
105 RCP8.5 scenario used by Giorgi et al. (2014b), along with their ensemble average. The first number in
106 parentheses shows the corresponding mean global precipitation change per degree of global warming, while the
107 second shows (for a subset of models with available data) the same quantity for global surface evaporation. The
108 annual precipitation is normalized by the mean precipitation during the reference period 1981–2010, therefore a
109 value of, e.g., 1.1 indicates an increase of 10%.

110

111 Although precipitation increases globally, at the regional level we can find relatively
112 complex patterns of change, with areas of increased and areas of decreased precipitation.
113 These patterns are closely related to changes in global circulation features, local forcings (e.g.
114 topography, land use) and energy and water fluxes affecting convective activity. The basic
115 geographical structure of precipitation change patterns has been quite resilient throughout
116 different generations of GCM projections, at least in an ensemble averaged sense. These



117 precipitation change patterns are shown in Figure 2 as obtained from the CMIP5 ensemble,
118 but they are similar in the CMIP3 and earlier GCM ensembles.



119 **Figure 2.** Ensemble mean change in precipitation (RCP8.5, 2071-2100 minus 1981-2010) for
120 December-January-February (panel a) and June-July-August (panel b) in the CMIP5 ensemble of models.

121 The patterns of Figure 2 have been often referred to as "the rich get richer and the poor
122 get poorer" in the sense that mid and high latitude regions, the Intertropical Convergence
123 Zone (ITCZ) and some tropical monsoon regions, which are already wet in present climate
124 conditions, are projected to become wetter with global warming, while dry sub-tropical
125 regions are projected to become drier.

126 The increase in precipitation at mid to high latitudes has been attributed to a poleward
127 shift of the storm tracks associated with maximum warming in the tropical troposphere (due
128 to enhanced convection), which in turn produces a poleward shift of the maximum horizontal
129 temperature gradient and jet stream location (e.g. IPCC 2013). This process is essentially
130 equivalent to a poleward expansion of the Hadley Cell, which also causes drier conditions in
131 sub-tropical areas, including the Mediterranean and Central America/Southwestern U.S.
132 regions. Conversely, the increase in precipitation over the ITCZ is due to increased
133 evaporation over the equatorial oceans, which feeds and intensifies local convective systems.
134 Finally, over monsoon regions, a general increase of precipitation has been attributed to the



135 greater water-holding capacity of the atmosphere that counterbalances a decrease in monsoon
136 circulation strength (IPCC 2013).

137 As already mentioned, these broad scale change patterns have been confirmed by
138 different generations of GCM projections, and thus appear to be robust model-derived signals.
139 On the other hand, high resolution RCM experiments have shown that local forcings
140 associated with complex topography and coastlines can substantially modulate these large
141 scale signals, often to the point of being of opposite sign. For example, the precipitation
142 shadowing effect of major mountain systems tends to concentrate precipitation increases
143 towards the upwind side of the mountains, and to reduce the increases or even generate
144 decreases of precipitation in the lee side (e.g. Giorgi et al. 1994; Gao et al. 2006). Similarly, in
145 the summer, the precipitation change signal can be strongly affected by high elevation
146 warming and wetting which enhance local convective activity. For example, Giorgi et al.
147 (2016) found enhanced precipitation over the Alpine high peaks in high resolution EURO-
148 CORDEX (Jacob et al. 2014) and MED-CORDEX (Ruti et al. 2016) projections, whereas the
149 driving coarse resolution global models produced a decrease in precipitation. In addition to
150 these local effects, it has been found that the simulation of some modes of variability, such as
151 blocking events, is also sensitive to model resolution (e.g. Anstey et al. 2013, Schiemann et al.
152 2017). As a result of all these processes it is thus possible that the "rich get richer, poor get
153 poorer" patterns might be significantly modified as we move to substantially higher resolution
154 models.

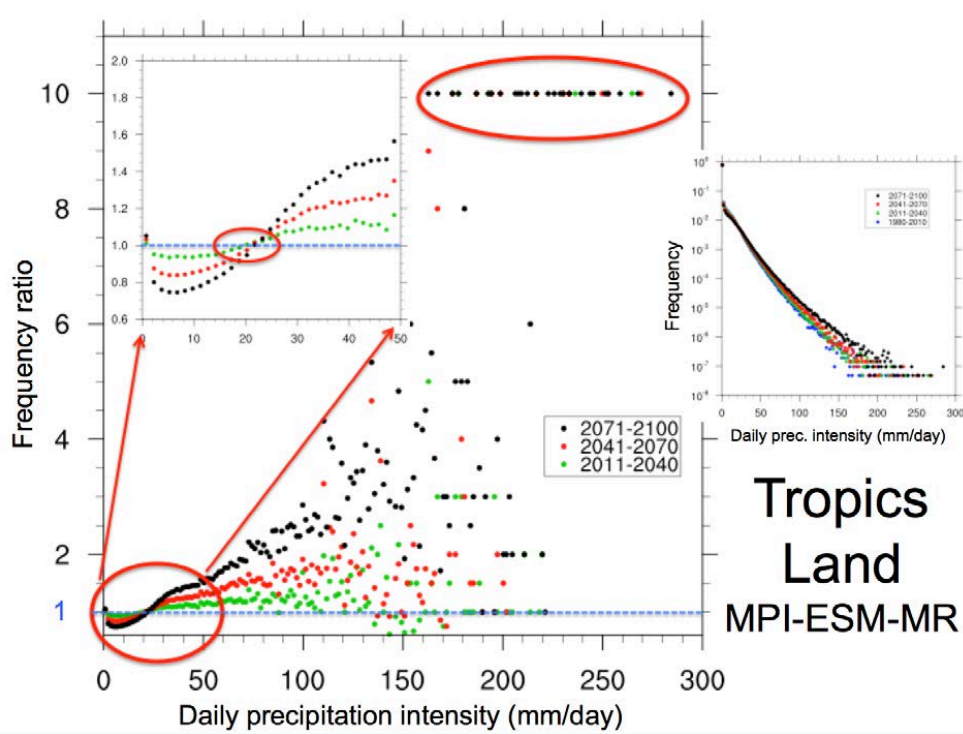
155 On the other hand, the question could be posed: "How richer will the rich get and how
156 poorer will the poor get?". This question depends more on the modifications of the
157 characteristics of precipitation than the mean precipitation itself. For example, changes in
158 precipitation interannual variability may have strong impacts on crop planning. As another
159 example, if an increase in precipitation is due to an increase of extreme damaging events, this



160 will have negative rather than positive impacts. Alternatively, if the increase is due to very
161 light events that do not replenish the soil of moisture, this will not constitute an added water
162 resource. Conversely, if a reduction of precipitation is mostly associated with a reduction of
163 extremes, then this will result in positive impacts. It is thus critical to assess how the
164 characteristics of precipitation will respond to global warming, which is the focus of the next
165 sections.

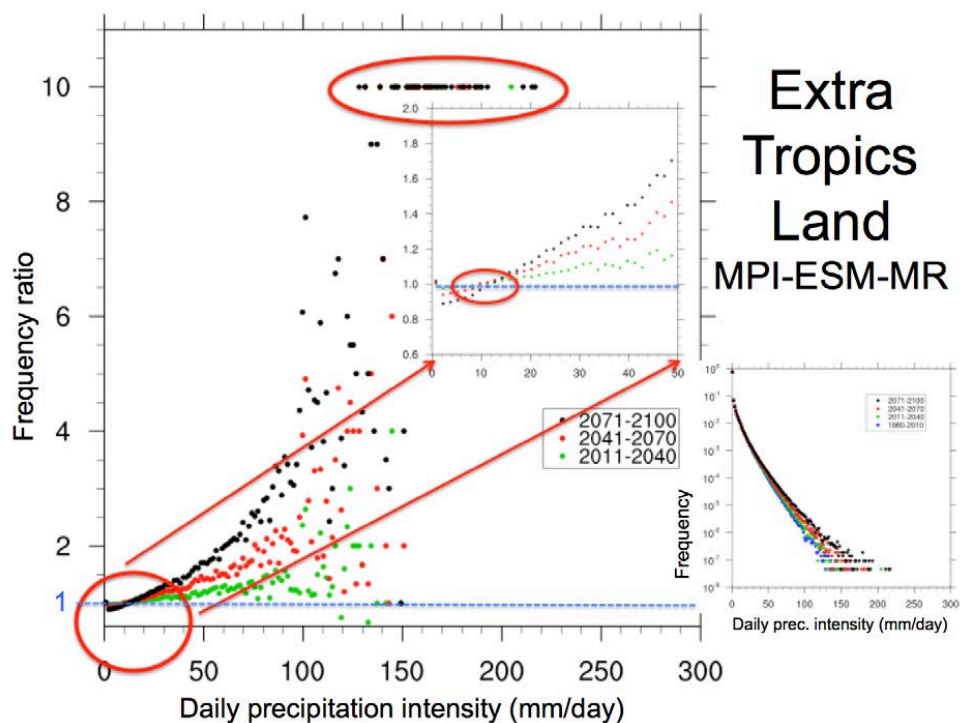
166 ***2.2 Daily precipitation intensity Probability Density Functions (PDFs)***

167 Daily precipitation is one of the variables most often used in impact assessment
168 studies, therefore an effective way to investigate the response of precipitation characteristics to
169 global warming is to assess changes in daily precipitation intensity PDFs. As an illustrative
170 example of PDF changes, Figures 3 and 4 show normalized precipitation intensity PDFs for 4
171 time slices, 1981-2010 (reference period representative of present day conditions), 2011-2040,
172 2041-2070 and 2071-2100 in the MPI-ESM-MR RCP8.5 projection of the CMIP5 ensemble.
173 The farther the time slice is in the future, the greater the warming (up to a maximum of about
174 4 °C in 2071-2100). The variable shown, which we refer to as PDF, is the frequency of
175 occurrence of precipitation events within a certain interval (bin) of intensity normalized by the
176 total number of days, including non-precipitating days, where a day is considered to be rainy
177 if the daily precipitation intensity is above 1 mm/day (as in Giorgi et al. 2014b). Given the
178 logarithmic scale of the frequency of occurrence, in order to better illustrate changes in
179 frequencies, the figure reports the ratio of the frequency of occurrence for a given bin in a
180 future time slice divided by the same quantity in the reference period. Finally, averaged data
181 are shown for land areas in the tropics (30°S-30°N, Figure 3), and extra-tropical midlatitudes
182 (30-60° N and S, Figure 4), noting that qualitatively similar results were found for ocean
183 areas.



184 **Figure 3.** Small right panel: Probability density function (PDF) defined as the normalized frequency of
 185 occurrence of daily precipitation events of intensity within a certain bin interval over land regions in the tropics
 186 (30°S - 30°N) for the reference period 1981-2010 and three future time slices (2011-2040, 2041-2070, 2071-
 187 2100) in the MPI-ESM-MR model. The frequency is normalized by the total number of days (including dry days,
 188 i.e. days with precipitation lower than 1 mm/day). Large central panel: Ratio of future to reference normalized
 189 frequency of daily precipitation intensity for the three future time slices. The small inset panel shows a zoom on
 190 the part of the curves highlighted by the corresponding red oval. Ratio values of 10 (highlighted in a red oval) are
 191 used when events occur in the future time slice which are not present in the reference period for a given intensity
 192 bin.

193



194

195 **Figure 4.** Same as Figure 3 but for extra-tropical land areas.

196

197 The PDFs exhibit a log-linear relationship between intensities and frequencies, with a
198 sharp drop in frequency as the intensity increases. The ratios of future vs. present day
199 frequencies consistently show the following features:

200 i) An increase in the number of dry days, as seen from the ratios > 1 in the first bin
201 (precipitation less than 1 mm/day), i.e. a decrease in the frequency of wet events. Note that,
202 even if these ratios are only slightly greater than 1, because the frequencies of dry days are
203 much higher than those of wet days, the actual absolute increase in the number of dry days is
204 relatively high.

205 ii) A decrease (ratio < 1) in the frequency of light to medium precipitation events up to
206 a certain intensity threshold. In the models we analyzed, when taken over large areas, this



207 threshold lies around the 95th percentile of the full distribution, and is higher for tropical than
208 extratropical land regions because of the higher amounts of precipitation in tropical
209 convection systems. Interestingly, while the threshold depends on latitude, it is approximately
210 invariant for all future time slices, i.e. it appears to be relatively independent of the level of
211 warming. The decrease in light precipitation events has been at least partially attributed to an
212 increase in thermal stability induced by the GHG forcing (Chou et al. 2012).

213 iii) An increase (ratio > 1) in the frequency of events for intensities higher than the
214 threshold mentioned above. The relative increase in frequency grows with the intensity of the
215 events, and it is thus maximum for the highest intensity events, an indication of a non linear
216 response of the precipitation intensity to warmer conditions. Note that, because of the
217 logarithmic frequency scale, the absolute increase in the number of high intensity events is
218 relatively low.

219 iv) The occurrence in the future time slices of events with intensity well beyond the
220 maximum found in the reference period. These are illustrated by the prescribed value of 10
221 when events occurred for a given bin in the future time slice, but not in the reference one. One
222 could thus interpret these as occurrences of "unprecedented" events.

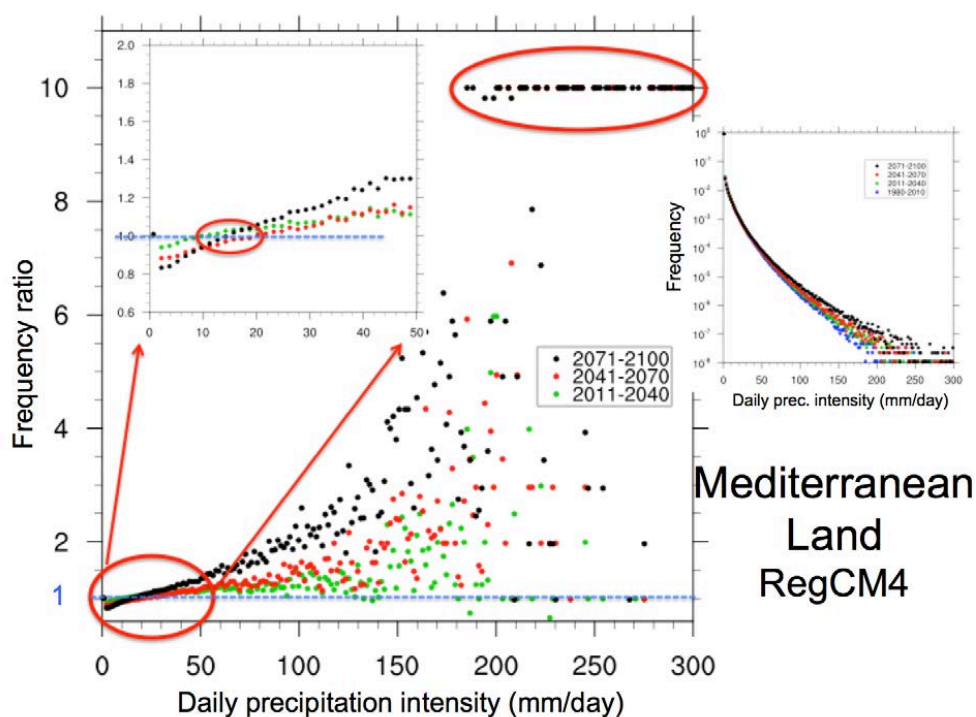
223 v) All the features i)-iv) tend to amplify as the time slice is further into the future, i.e.
224 as the level of warming increases, and are generally more pronounced over tropical than
225 extratropical areas (and over land than ocean regions, which we did not show for brevity).

226 Although the results in Figures 3 and 4 are obtained from one model, they are
227 qualitatively consistent with those we found for other CMIP5 GCMs (not shown for brevity).
228 We also carried out the same type of analysis for a high resolution RCM projection (12 km
229 grid spacing, RCP8.5 scenario) conducted with the RegCM4 model (Giorgi et al. 2012) over
230 the Mediterranean domain defined for the MED-CORDEX program (Ruti et al. 2016).
231 Figures 5 and 6 show PDFs and PDF ratios for three 30-year future time slices calculated over



232 land areas throughout the Mediterranean domain and over a sub-area covering the Alpine
233 region. They show features similar to those found for the GCMs, with the signal over the
234 Alpine region being more pronounced than for the entire Mediterranean area. In addition, our
235 results are qualitatively in line with previous analyses of RCM projections (e.g. Gutowski et
236 al. 2007; Boberg et al. 2009; Jacob et al 2014; Giorgi et al. 2014a), suggesting that the
237 projected changes in precipitation intensity PDFs summarized in the points i)-iv) above are
238 generally robust across a wide range of models and model resolutions.

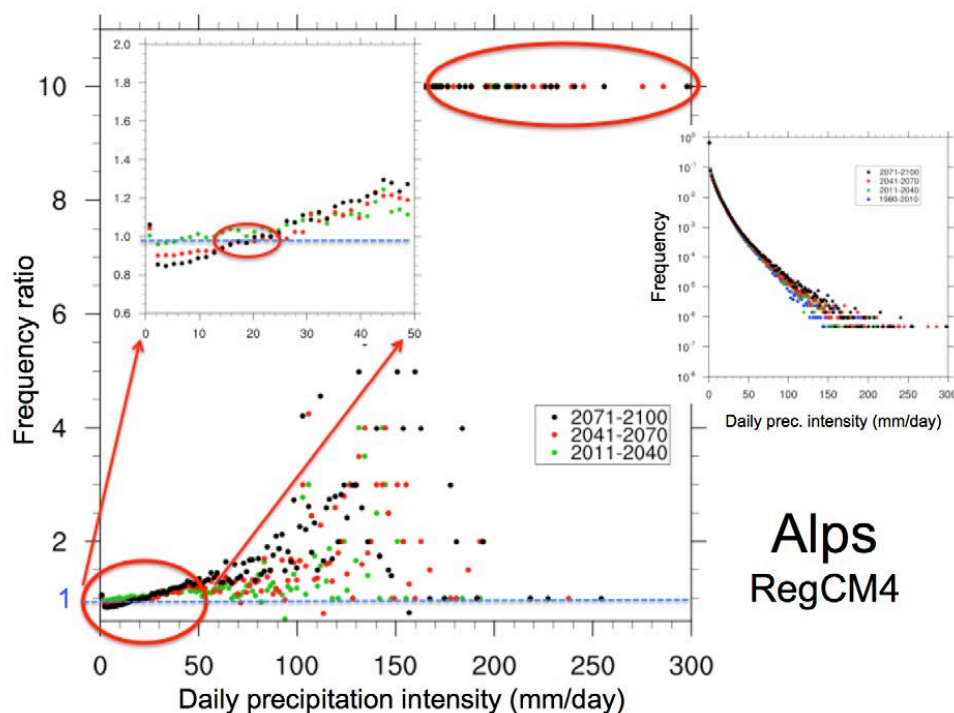
239



240

241 **Figure 5.** Same as Figure 3 but for Mediterranean land areas in a MED-CORDEX experiment with the
242 RegCM4 RCM driven by global fields from the HadGEM GCM.

243



Alps
RegCM4

244

245 **Figure 6.** Same as Figure 5 but for the Alpine region.

246

247 **2.3 Hydroclimatic indices**

248 The changes in precipitation intensity PDFs found in the previous section should be
249 reflected in, and measured by, changes of hydroclimatic indices representative of given
250 precipitation regimes. In two previous studies (Giorgi et al. 2011, 2014b), we assessed the
251 changes of a series of interconnected hydroclimatic indices in an ensemble of 10 CMIP5
252 projections. The indices analyzed include:

253 SDII: Mean precipitation intensity (including only wet events)

254 DSL: Mean dry spell length, i.e. mean length of consecutive dry days

255 WSL: Mean wet spell length, i.e. mean length of consecutive wet days



256 R95: Fraction of total precipitation above the 95th percentile of the daily precipitation
257 intensity distribution during the reference period 1981-2010.

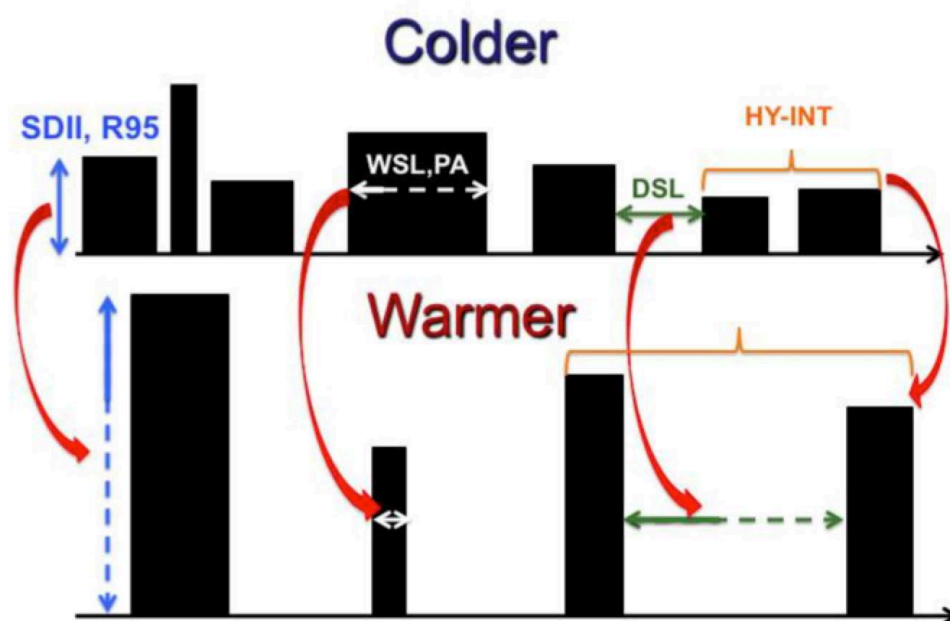
258 PA: Precipitation area, i.e. the total area covered by wet events at any given day

259 HY-INT, i.e. the hydroclimatic intensity index introduced by Giorgi et al. (2011)
260 consisting of the product of normalized SDII and MDSL.

261 Note that the PA and HY-INT indices were specifically introduced by Giorgi et al.
262 (2011, 2014b). The PA is the spatial counterpart of the mean frequency of precipitation days,
263 while the HY-INT was introduced under the assumption that the changes in SDII and MDSL
264 are interconnected responses to global warming (Giorgi et al. 2011).

265 Giorgi et al. (2011, 2014b) examined changes in these indices for ensembles of
266 CMIP3 and CMIP5 GCM projections, as well as a number of RCM projections, in future time
267 slices with respect to the 1976-2005 reference period. Their results, which were consistently
268 found for most models analyzed, are schematically depicted in Figure 7, which shows that
269 under warming conditions the models indicate a prevalent increase in SDII, R95, HY-INT and
270 DSL and a decrease in PA and WSL. Similar results were then found by Giorgi et al. (2014a)
271 in an analysis of multiple RegCM4-based projections over 5 CORDEX domains. In other
272 words, under warmer climate conditions, precipitation events are expected to be more intense
273 and extreme and temporally more concentrated and less frequent, which implies a reduction
274 of the areas occupied by rain at any given time (although not necessarily a reduction of the
275 size of the events). This conclusion is consistent with the change in PDFs illustrated in
276 Figures 3-6.

277



278

279 **Figure 7.** Schematic depiction of the hydroclimatic response to climate warming emerging from the
280 analysis of multiple indices by Giorgi et al. (2014b), which showed an increase in SDII, R95, HY-INT and DSL
281 and a decrease in PA and WSL. Each box represents a precipitation event whose area is the total amount of
282 precipitation, the height is the intensity and the horizontal length the duration. The interval between two events
283 represents a dry period.

284 In addition, Giorgi et al. (2011 and 2014b) analyzed a global and several regional daily
285 precipitation gridded observation datasets, and found that trends for the period 1976-2005
286 were predominantly in line with the changes illustrated in Figure 7 over most continental
287 areas. Further evidence of increases in heavy precipitation events in observational records is
288 for example reported by Fischer and Knutti (2016) and references therein, however this
289 conclusion cannot be considered entirely robust, and needs to be verified with further
290 analysis, due to the high uncertainty in precipitation observations (e.g. Herold et al. 2017).

291 An explanation for the hydroclimatic response to global warming illustrated in Figure
292 7 is related to the fact that, on the one hand, the mean global precipitation change roughly



293 follows the mean global evaporation increase, i.e. 1.5-2.0 %/DGW (Trenberth et al. 2007,
294 Figure 1), while, on the other hand the intensity of precipitation, in particular for high and
295 extreme precipitation events, is more tied to the increase in the water holding capacity of the
296 atmosphere, which is in turn regulated by the Clausius-Clapeyron (Cl-Cl) response of about
297 7%/DGW (e.g. Trenberth et al. 2003; Pall et al. 2007; Lenderink and van Meijgaard 2008;
298 Chou et al. 2012; Singleton and Toumi 2013; Ivancic and Shaw 2016; Fischer and Knutti
299 2016). Therefore the increase in precipitation intensity can be expected to be larger than the
300 increase in mean precipitation, which implies a decrease in precipitation frequency.

301 To illustrate this point, Table 1 reports the globally averaged changes (2071-2100
302 minus the reference period 1976-2005, as in Giorgi et al. 2014b; RCP8.5 scenario) in mean
303 precipitation, precipitation intensity and frequency, and 95th, 99th and 99.9th percentile of
304 daily precipitation for the 10 GCMs of Giorgi et al. (2014b), along with their ensemble
305 average. The values of Table 1 were calculated as follows: we first computed the change in
306 %/DGW at each model grid point and then averaged these values over global land+ocean as
307 well as global land-only areas. This was done in order to avoid the possibility that areas with
308 large precipitation amounts may dominate the average. On the other hand, grid-point
309 normalization artificially amplifies the contribution of regions with small precipitation
310 amounts, such as polar and desert areas. For this reason, as in Giorgi et al. (2014), we did not
311 include in the averaging areas north of 60°N and south of 60 °S (polar regions) along with
312 areas with mean annual precipitation lower than 0.5 mm/day (which effectively identifies
313 desert regions). In addition, we did not consider precipitation associated with days with
314 amounts of less than 1 mm/day in order to be consistent with our definition of rainy day
315 (which disregards drizzle events).



Global Box						
Models	N. Wet Days %/ DGW	Precipitation change (due to wet days)%/ DGW	SDII change(%)/ DGW	95p change(%)/ DGW	99p change(%)/ DGW	99.9p change(%)/ DGW
HadGEM-ES	-0.7	1.3	1.8	1.7	2.9	3.9
MPI-ESM-MR	-2.4	1.0	3.5	1.9	3.7	5.3
GFDL-ESM2M	-1.4	0.05	1.2	0.3	2.1	10.4
IPSL-CM5A-MR	-1.0	1.6	2.6	2.0	4.5	7.9
CCSM4	-1.1	0.7	1.8	1.1	2.8	5.5
CanESM2	-0.4	1.6	1.7	1.5	2.5	4.4
EC-EARTH	-0.9	1.3	2.1	1.9	3.7	5.9
MIROC-ESM	0.2	1.4	0.9	1.1	1.2	1.6
CSIRO-Mk3-6-0	-0.6	0.8	1.9	2.3	2.4	3.4
CNRM-CM5	-0.1	1.4	1.5	1.5	2.9	5.8
ENSEMBLE	-0.8	1.1	1.9	1.5	2.9	5.4

Global LAND Box						
Models	N. Wet Days %/ DGW	Precipitation change (due to wet days)%/ DGW	SDII change(%)/ DGW	95p change(%)/ DGW	99p change(%)/ DGW	99.9p change(%)/ DGW
HadGEM-ES	-1.4	0.7	2.1	1.2	2.8	4.5
MPI-ESM-MR	-3.3	0.1	4.0	0.8	3.7	5.4
GFDL-ESM2M	-1.8	1.1	3.1	1.2	4.5	12.4
IPSL-CM5A-MR	-1.8	0.7	2.5	1.2	3.8	7.2
CCSM4	-0.6	1.3	1.9	1.3	2.8	5.4
CanESM2	-0.6	1.2	1.7	1.3	3.4	5.0
EC-EARTH	-0.8	1.4	2.3	2.0	3.8	6.0
MIROC-ESM	0.2	1.8	1.4	1.1	1.7	2.1
CSIRO-Mk3-6-0	-1.8	-0.2	1.5	0.2	1.1	2.4
CNRM-CM5	0.4	2.5	2.0	2.0	3.2	6.0
ENSEMBLE	-1.2	1.1	2.3	1.2	3.1	5.6

316 **Table 1.** Change in different daily precipitation indicators between 2071-2100 and 1976-2005 for the 10
 317 CMIP5 GCMs of Giorgi et al. (2014b) expressed in % per degree of surface global warming over global (upper
 318 box) and global-land (lower box) areas, where global means the area between 60°S and 60°N. SDII is the
 319 precipitation intensity, 95p, 99p and 99.9p are the 95th, 99th and 99.9th percentiles, respectively, and the
 320 precipitation change only include wet days, i.e. days with precipitation greater than 1 mm/day.

321

322 Also in these calculations, the increase in global mean precipitation is in the range of
 323 1-2 %/DGW except for the GFDL experiment, which shows a very small increase (indicating
 324 that in this model most of the precipitation increase occurs in the polar regions). In all cases
 325 except for MIROC the increase in global SDII is greater than the increase in mean



326 precipitation, resulting in a decrease of the number of rainy days. The changes in the 95th,
327 99th and 99.9th percentile are maximum for the most extreme percentiles, showing that the
328 main contribution to the response of Figure 7 is due to the highest intensity events, i.e. above
329 the 99th and 99.9th percentiles, whose response becomes increasingly closer to the CI-CI one.
330 In fact, the increase in 95th percentile for the ensemble model average is lower than the
331 increase in SDII, and this is because in some models the threshold intensity in Figures 3-6,
332 where the sign of the change turns from negative to positive, lies beyond the 95th percentile.
333 When only land areas between 60°S and 60°N are taken into account (bottom panel in Table
334 1), the changes are generally in line with the global ones, except for the CNRM model. Over
335 land areas we also find changes in the highest percentiles of magnitude mostly greater than
336 over the globe (and thus over oceans).

337 We can thus conclude that the shift to a regime of more intense but less frequent
338 events in warmer conditions is due to the fact that precipitation intensity, especially for
339 intense events (beyond the 95th percentile), responds at the local level primarily to the CI-CI-
340 driven increase of water vapor amounts, while mean precipitation responds to a slower
341 evaporation process, driving a decrease in precipitation frequency. Noticeably, the MIROC
342 experiment does not appear to follow this response, i.e. in this model the increase in mean
343 precipitation appears to be driven by an increase in the number of light precipitation events.

344 While the data of Table 1 provide a diagnostic explanation of the hydroclimatic
345 response of Figure 7, it has also been suggested by very high resolution convection-permitting
346 simulations that ocean temperatures might affect the self-organization and aggregation of
347 convective systems (e.g. Mueller and Held 2012; Becker et al. 2017), which would also affect
348 the precipitation response to warming. Therefore, the study of this response might lead to a
349 greater understanding of the fundamental behavior of the precipitation phenomenon, and in
350 particular of tropical convection processes.



351 **3. Some consequences of the hydroclimatic response to global warming**

352 What are the consequences of the "more intense, less frequent" event response to
353 global warming illustrated in Figure 7? Obviously there can be many of them, but here we
354 want to provide a few illustrative examples of relevance for impact applications.

355 ***3.1 Potential stress associated wet and dry extreme events.***

356 Figure 7 suggests that global warming might induce an increase in the risk of
357 damaging extreme wet and dry events, the former being associated with the increase in
358 precipitation intensity, and latter with the occurrence of longer sequences of dry days over
359 areas of increasing size. In order to quantify this risk, in a recent paper (Giorgi et al. 2018,
360 hereafter referred to as GCR18) we introduced a new index called the Cumulative
361 Hydroclimatic Stress Index, or CHS. In GCR18, the CHS was calculated for two types of
362 extreme events, the 99.9th percentile of the daily precipitation distribution (or R99.9) and the
363 occurrence of at least three consecutive months experiencing a precipitation deficit of
364 magnitude greater than 25% of the precipitation climatology for that months (or D25). Both of
365 these metrics thus refer to extremely wet and dry events which can be expected to produce
366 significant damage (see GCR18).

367 Taking as an example the R99.9, the CHS essentially cumulates the excess
368 precipitation above the 99.9th percentile threshold calculated for a given reference period (e.g.
369 1981-2010). Hence, the assumption is that the potential stress associated with these extremes
370 is proportional to the excess precipitation above the 99.9 percentile of the distribution. GCR18
371 calculated this quantity for a future climate projection, and then normalized it by the
372 corresponding value cumulated over the reference period. This normalization expresses the
373 potential stress due to the increase in wet extremes in Equivalent Reference Stress Years
374 (ERSY), where an ERSY is the mean stress per year due to the extremes during the reference

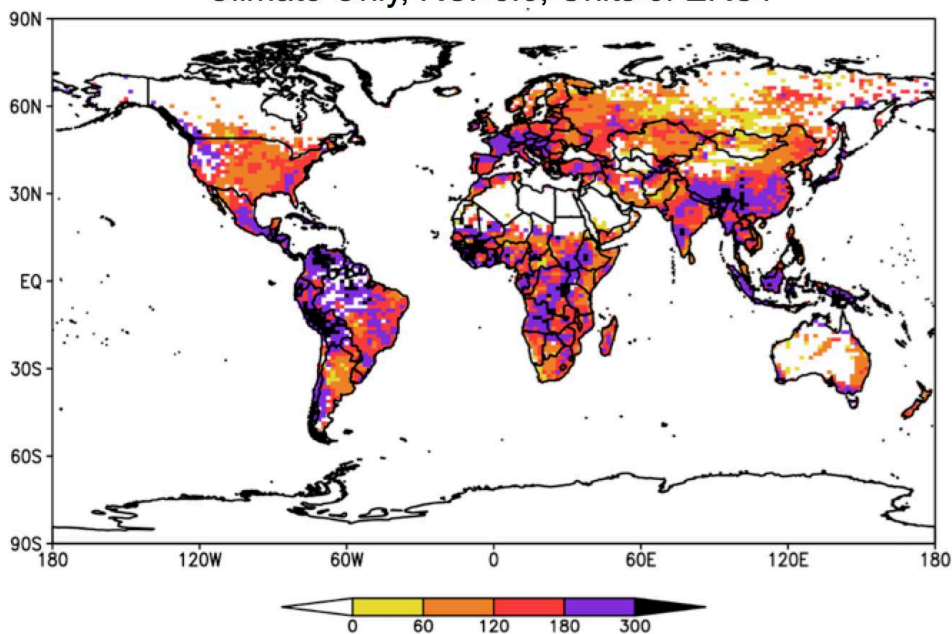


375 period (in our case 1981-2010). If, for example, a damage value can be associated to such
376 events, the ERSY can be interpreted as the mean yearly damage caused by extremes in
377 present climate conditions. GCR18 then carried out similar calculations for the cumulative
378 potential stress due to dry events by cumulating the deficit rain defined by the D25 metric. In
379 addition, they included exposure information within the definition of the CHS index by
380 multiplying the excess or deficit precipitation by future population amounts (as obtained from
381 Shared Socioeconomic Pathways, or SSP, Rihai et al. 2016) normalized by present day
382 population values. The details of these calculations can be found in GCR18.

383 The main results of GCR18 are summarized in Figures 8 and 9, which present maps of
384 the potential cumulative stress due to both dry and wet events added by climate change during
385 the period 2010-2100 and expressed in added ERSY (i.e. after removing the value of 90 that
386 would be obtained if no climate change occurred). The figures show the total ensemble-
387 averaged added cumulative stress for the RCP8.5 scenario without (Figure 8) and with (Figure
388 9) inclusion of population weighting (where the SSP5 population scenario from Rihai et al.
389 2016 was used).



Additional Cumulative Hydroclimatic Stress by 2100 Climate Only, RCP8.5, Units of ERSY

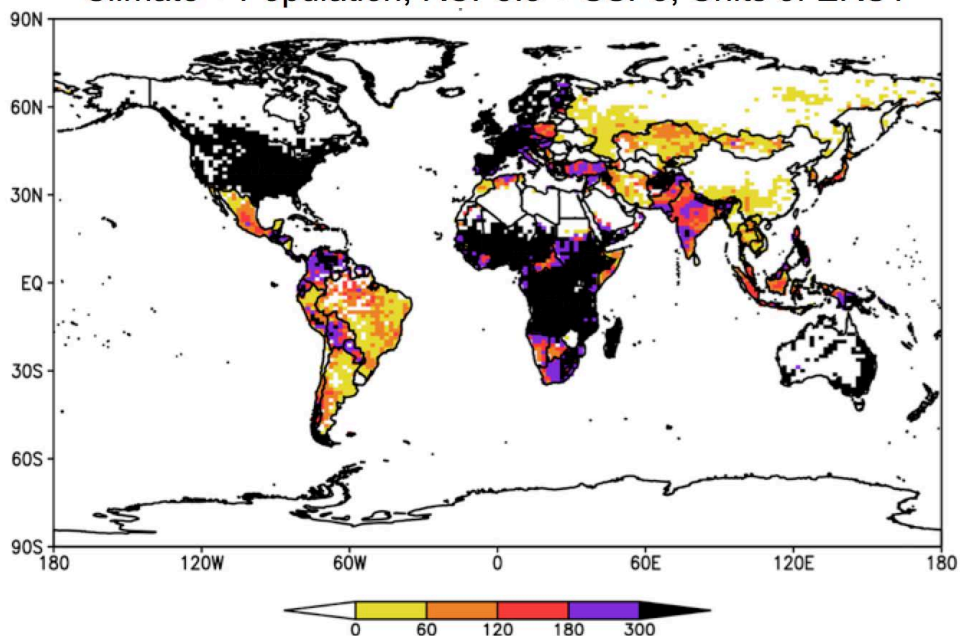


390 **Figure 8.** Total number of additional stress years due to increases in wet (R99.9) and dry (D25) events
391 for the period 2011 - 2100 including only climate variables for the RCP8.5 scenario (see text for more detail).
392 Units are Equivalent Reference Stress Years (ERSY) and the value does not include ERSY obtained if climate
393 did not change (i.e. for the period 2100 - 2011 a value of 90).

394



Additional Cumulative Hydroclimatic Stress by 2100 Climate + Population, RCP8.5 + SSP5, Units of ERSY



395

396 **Figure 9.** Same as Figure 8, but with the inclusion of the SSP5 population scenario (see text for more
397 detail).

398

399 Figure 8 shows that, when only climate is accounted for, dry and wet extremes add
400 more than 180 ERSY (and in some cases more than 300 ERSY) over extended areas of
401 Central and South America, Europe, Western and south/central Africa, Southern and
402 Southeastern Asia. In other words, the combined potential stress due to dry and wet extremes
403 more than triples due to climate change by the end of the century. In this regard, GCR18
404 found that, when globally averaged over land regions and over all the models considered, both
405 wet and dry extremes increased in the RCP8.5 scenario, the former adding ~120 ERSY, while
406 the latter adding ~30 ERSY.



407 When population scenarios are also accounted for (Figure 9) the patterns of added
408 cumulative stress are considerably modified. In this case, the total number of added ERSY
409 exceeds 300 over the entire continental U.S. and Canada, most of Africa, Australia and areas
410 of South and Southeast Asia, which are projected to experience substantial population increases
411 in the SSP5 scenario. Conversely, we find a reduced increase in stress over East and Southeast
412 Asia, where population is actually projected to decrease by the end of the 21st century (see
413 GCR18). This result thus points to the importance of incorporating socio-economic
414 information in the assessment of the stress associated with climate change-driven extreme
415 events.

416 Notwithstanding the limitations and approximations of the approach of GCR18, amply
417 discussed in that paper, the results of Figures 8 and 9 clearly indicate that the increase of wet
418 and dry extremes associated with global warming can constitute a serious threat to the socio-
419 economic development of various regions across all continents. GCR18 also show that the
420 cumulative stress due to increases in extremes is drastically reduced under the RCP2.6
421 scenario, pointing to the importance of mitigation measures to reduce the level of global
422 warming.

423 ***3.2 Impact on interannual variability.***

424 The interannual variability of precipitation is a key factor affecting many aspects of
425 agriculture and water resources and it is strongly affected by global modes of variability, such
426 as the El Niño Southern Oscillation (ENSO) in the tropics and the North Atlantic Oscillation
427 (NAO) in mid-latitudes. In this regard, the latest generation of GCM projections does not
428 provide strong indications concerning changes in the frequency or intensity of such modes
429 (e.g. IPCC 2013).



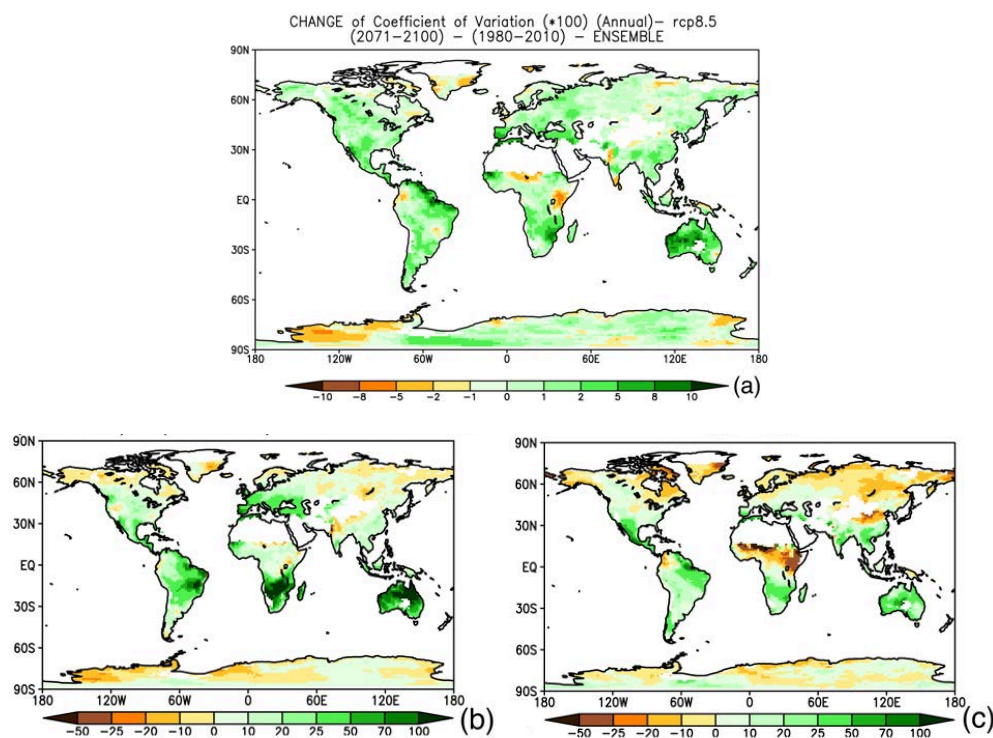
430 Daily and seasonal precipitation statistics are not necessarily tied, since the same
431 seasonal mean can be obtained via different sequences of daily precipitation events. In
432 addition, the intensity distribution of daily and seasonal precipitation amounts can be quite
433 different, the latter being often close to normal distributions (e.g. Giorgi and Coppola 2009).
434 On the other hand, the occurrence of longer dry spells, intensified by higher temperatures and
435 lower soil moisture amounts, might be expected to amplify dry seasons, while the increase in
436 the intensity of sequences of wet events might lead to amplified wet seasons. As a result, it
437 can be expected that the regime response of Figure 7 might lead to an increase in precipitation
438 interannual variability.

439 To verify this hypothesis, we calculated for the GCM ensemble of Giorgi et al.
440 (2014b) the change in precipitation interannual variability between future and present day 30-
441 year time slices using as metric the coefficient of variation (CV). The CV is defined as the (in
442 our case interannual) standard deviation normalized by the mean, and has been often used as a
443 measure of precipitation variability because it removes the strong dependence of precipitation
444 variability on the mean itself (Raisanen 2002; Giorgi and Bi 2005).

445



446



447 **Figure 10.** Change in precipitation interannual coefficient of variation (2071-2100 vs. 1981-2010) for a)
448 mean annual precipitation; b) April-September precipitation; c) October-March precipitation.

449

450 Figure 10 shows the ensemble average change in precipitation CV between the 2071-
451 2100 and 1981-2010 time slices for mean annual precipitation as well as precipitation
452 averaged over the two 6-month periods Apr-Sept and Oct-Mar. It can be seen that, when
453 considering annual averages, the interannual variability increases over the majority of land
454 areas, with exceptions over small regions scattered throughout the different continents. When
455 considering the two different 6-month seasons, in Apr-Sept (northern hemisphere summer,
456 southern hemisphere winter) variability increases largely dominate, except over areas of the
457 northern hemisphere high latitudes and some areas around major mountain systems. In Oct-



458 Mar, the areas of decreased variability are more extended over northern Eurasia, northern
459 North America and, interestingly, some equatorial African regions, although still the increases
460 are somewhat more widespread.

461 Although Figure 10 does not show a signal of ubiquitous sign across all land areas, it
462 clearly points to a prevalent increase in interannual variability associated with global
463 warming, at least as measured by the CV. It is important to notice that this increase occurs in
464 areas of both increased and decreased mean precipitation (see Figure 2), so that it is not
465 strongly related to the use of the CV as a metric. Finally, this result is broadly consistent with
466 analyses of previous generation model projections (Raisanen 2002; Giorgi and Bi 2005),
467 which adds robustness to this conclusion.

468 ***3.2 Impact on precipitation predictability.***

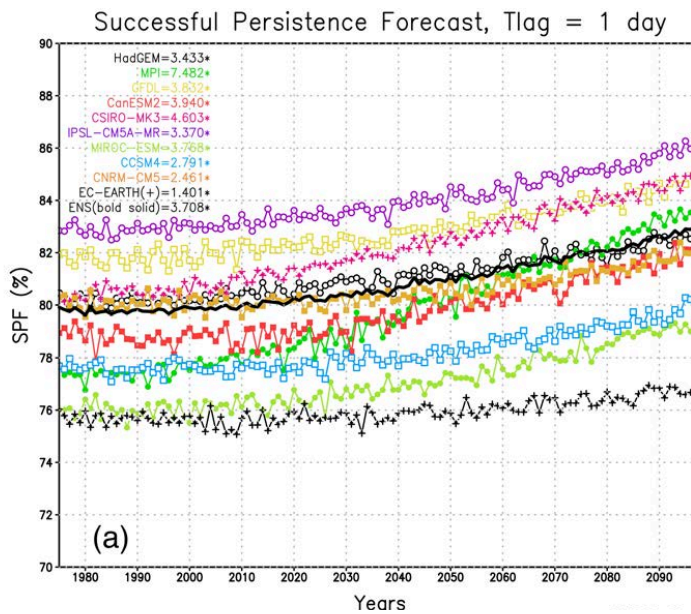
469 A third issue we want to address concerns the possible effects of regime shifts on the
470 predictability of precipitation, an issue which has obvious implications for a number of socio-
471 economic activities (e.g. agriculture, hazards, tourism etc.). Indeed, precipitation is one of the
472 most difficult meteorological variables to forecast, since it depends on both large scale and
473 complex local scale processes (e.g. topographic forcing). While the chaotic nature of the
474 atmosphere provides a theoretical limit to weather prediction of ~10-15 days (e.g. Warner
475 2010), the predictability range of different types of precipitation events depends crucially on
476 the temporal scale of the dynamics related to the event itself. For example, the predictability
477 range of synoptic systems is of the order of days, while that of long-lasting weather regimes,
478 such as blockings, can be of weeks. It is thus clear that changes in precipitation regimes and
479 statistics can lead to changes in the potential predictability of precipitation.

480 One of the benchmark metrics that is most often used to assess the skill of a prediction
481 system is persistence (Warner 2010). Essentially, persistence for a lead time T assumes that a



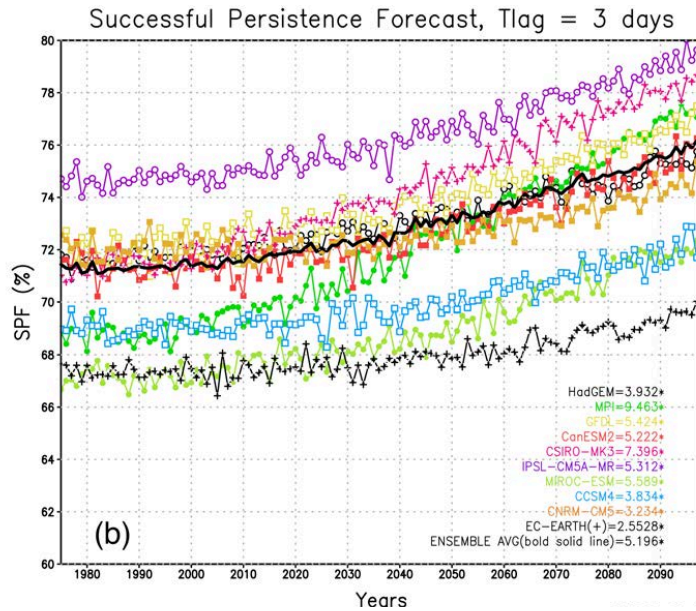
482 given weather condition at a time $t+T$ is the same as that at time t . In other words, when
483 applied for example to daily precipitation, it assumes that, for a lead time of N days, if day i is
484 wet (dry), day $i + N$, will also be wet (dry). The skill of a forecast system is then measured by
485 how much the forecast improves upon persistence. Therefore, persistence can be considered
486 as a "minimum potential predictability".

487 In order to assess whether global warming affects what we defined minimum potential
488 predictability for precipitation, we calculated the percentage of successful precipitation
489 forecasts obtained from persistence at lead times of 1, 3 and 7 days for the 10 GCM
490 projections (RCP8.5) used by Giorgi et al. (2014). This percentage, calculated year-by-year
491 and then averaged over all land areas, is presented in Figure 11, noting that the persistence
492 forecast only concerns the occurrence of precipitation and not the amount.

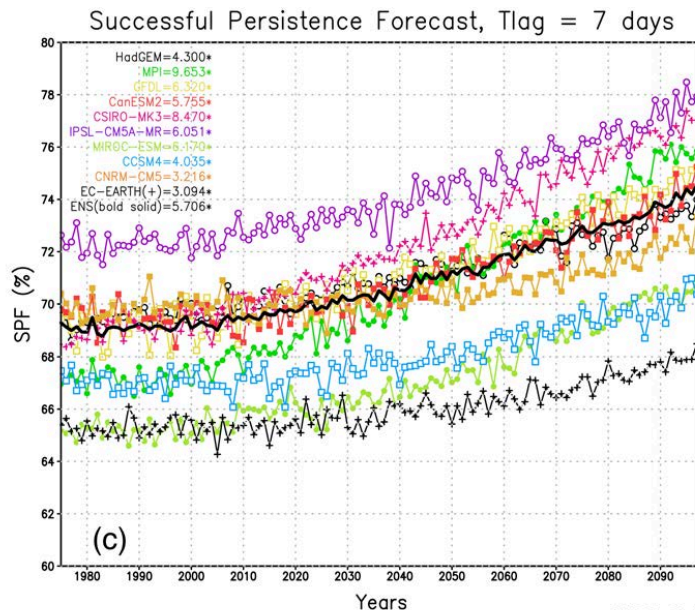


493

494



495



496

497 **Figure 11.** Fraction of successful forecasts as a function of time using persistence for daily
 498 precipitation occurrence at time lags of a) 1 day; b) 3 days; and c) 7 days, for the GCM ensemble of Giorgi et al
 499 (2014b) (bold black line). The number in parenthesis denotes the trend in % per 100 years. Units are percentage
 500 of days in one year for which persistence provides a successful forecast (either dry or wet).

501



502 Figure 11 shows that in all model projections, and thus in the ensemble averages, the
503 percent of successful persistence forecasts increases with global warming for all three time
504 lags. This can be mostly attributed to the increase in mean dry spell length found in section 2.
505 For a lag time of 1 day, the successful persistence forecast in the model ensemble increases
506 globally from about 80% in 2010 to about 83% in 2100, i.e. with a linear trend of $\sim 3.5\%/100$
507 yrs. As can be expected, the % of successful persistence forecasts decreases with the length
508 of lag time, $\sim 76\%$ and 69% on 2010 for lag times of 3 and 7 days, respectively. However the
509 growth rate of this percentage also increases with lag time, $5.2\%/100$ yrs and $5.7\%/100$ yrs for
510 lag times of 3 and 7 days, respectively.

511 Despite the simplicity of the reasoning presented in this section, our results indicate
512 that global warming can indeed affect (and in our specific case, increase) the potential
513 predictability of the occurrence of dry vs. wet days. For example, persistence for the 7 day lag
514 time has the same successful forecast rate by the middle of the 21st century as the present day
515 persistence for the 3 day lag time ($\sim 71\%$). Clearly, the issue of the effects of climate change
516 on weather predictability is a very complex one, with many possible implications not only
517 from the application point of view, but also for the assessment of the performance of forecast
518 systems. It is thus important that this issue is addressed with more advanced techniques and
519 metrics than we employed in our illustrative example.

520 **4. Concluding remarks**

521 In this paper we have revisited the basic responses of the characteristics of the Earth's
522 hydroclimatology to global warming through the analysis of global and regional climate
523 model projections for the 21st century. The projections examined suggested some robust
524 hydroclimatic responses, in the sense of being mostly consistent across different model



525 projections and being predominant over the majority of land areas. They can be summarized
526 as follows:

- 527 1) A decrease (increase) in the frequency of wet (dry) days
- 528 2) An increase in the mean length of dry spells
- 529 3) An increase of the mean intensity of precipitation events
- 530 4) An increase in the intensity and frequency of wet extremes
- 531 5) A decrease in the frequency of light to medium precipitation events
- 532 6) A decrease in the mean length of wet events and in the mean area covered by
533 precipitation
- 534 7) Occurrence of wet events of magnitude beyond that found in present climate
535 conditions

536 We discussed how this response is mostly tied to the different natures of the
537 precipitation and evaporation processes, and we also presented some illustrative examples of
538 the possible consequences of these responses, including an increase in the risks associated
539 with wet and dry extremes, a predominant increase in the interannual variability of
540 precipitation and a modification of the potential predictability of precipitation events. In
541 addition, some of the results 1)-7) above are consistent with previous analyses of global and
542 regional model projections (e.g. Tebaldi et al. 2006; Gutowski et al. 2007; Giorgi et al.
543 2011,2014a,b; Sillmann et al. 2013a).

544 Clearly, model projections indicate that the characteristics of precipitation are going to
545 be substantially modified by global warming, most likely to a greater extent than mean
546 precipitation itself. Whether these changes are already evident in the observational record is



547 still an open debate. Giorgi et al. (2011, 2014b) found some consistency between model
548 projections and observed trends in different precipitation indices for the period 1976 - 2005 in
549 a global and some regional observational datasets. Some indications of observed increases in
550 precipitation extremes over different regions of the World have also been highlighted in
551 different IPCC reports (IPCC 2007, 2013) and, for example, in Fischer and Knutti (2016). In
552 addition, data from the Munich reinsurance company suggest an increase in the occurrence of
553 meteorological and climatic catastrophic events, such as flood and drought, since the mid-
554 eighties. However, the large uncertainty and diversity in precipitation observational estimates,
555 most often blending in situ station observations and satellite-derived information using a
556 variety of methods, along with the paucity of data coverage in many regions of the World and
557 the large variability of precipitation, make robust statements on observed trends relatively
558 difficult.

559 A key issue concerning precipitation projections is the representation of cloud and
560 precipitation processes in climate models. These processes are among the most difficult to
561 simulate, because they are integrators of different physical phenomena and, especially for
562 convective precipitation, they occur at scales that are smaller than the resolution of current
563 GCMs and RCMs. For example, the representation of clouds and precipitation is the main
564 contributor to a model's climate sensitivity and the simulation of precipitation statistics is
565 quite sensitive to the use of different cumulus parameterizations (e.g. Flato et al. 2013). In
566 fact, both global and regional climate models have systematic errors in the simulation of
567 precipitation statistics, such as an excessive number of light precipitation events and an
568 underestimate of the intensity of extremes (Kharin et al. 2005; Flato et al. 2013, Sillmann et
569 al. 2013b). These systematic biases are related non only to the relatively coarse model
570 resolution, but also to inadequacies of resolvable scale and convective precipitation
571 parameterizations (e.g. Chen and Knutson 2008; Wehner et al. 2010; Flato et al. 2013).



572 Experiments with non-hydrostatic RCMs run at convection-permitting resolutions (1-3
573 km), in which cumulus convection schemes are not utilized and convection is explicitly
574 resolved with non-hydrostatic wet dynamics, have shown that some characteristics of
575 simulated precipitation are strongly modified compared to coarser resolution models, most
576 noticeably the precipitation peak hourly intensity and diurnal cycle (e.g. Prein et al. 2015). It
577 is thus possible that some conclusions based on coarse resolution models might be modified
578 as more extensive experiments at convection permitting scales become available.

579 Despite these difficulties and uncertainties, and given the problems associated with
580 retrieving accurate observed estimates of mean precipitation at continental to global scales,
581 robust changes in different characteristics of precipitation (rather than the mean) may provide
582 the best opportunity to detect and attribute trends in the Earth's hydrological cycle. Moreover,
583 the investigation of the response of precipitation to warming may provide an important tool
584 towards a better understanding and modeling of key hydroclimatic processes, most noticeably
585 tropical convection. The ability of simulating given responses of precipitation characteristics
586 can also provide an important benchmark to evaluate the performance of climate models in
587 describing precipitation and cloud processes. Therefore, as more accurate observational
588 datasets become available, along with higher resolution and more comprehensive GCM and
589 RCM projections, the understanding of the response of the Earth's hydroclimate to global
590 warming, and its impacts on human societies, will continue to be one of the main research
591 challenges within the global change debate.

592 **Acknowledgements**

593 We thank the CMIP5 and MED-CORDEX modeling groups for making available the
594 simulation data used in this work, which can be found at the web site [http://cmip-](http://cmip-pcmdi.llnl.gov/cmip5/data_portal.html)
595 [pcmdi.llnl.gov/cmip5/data_portal.html](http://cmip-pcmdi.llnl.gov/cmip5/data_portal.html) and <https://www.medcordex.eu/medcordex.php>. A



596 good portion of the material presented in this paper is drawn from the European Geosciences
597 Union (EGU) 2018 Alexander von Humboldt medal lecture delivered by one of the authors
598 (F.G.).

599

600 **Competing Financial Interests**

601 The authors declare no competing financial interests.

602

603 **References**

604 Allan, R.P., and Soden, B.J.: Atmospheric warming and the amplification of
605 precipitation extremes, *Science*, 321, 1481-1484, 2008.

606 Anstey, J.A., Davini, P., Grey, L.J., Woollings, T.J., Butchart, N., Cagnazzo, C.,
607 Christiansen, B., Hardiman, S.C., Osprey, S.M., and Yang, S. : (2013). Multi-model analysis
608 of northern hemisphere winter blocking: Model biases and the role of resolution, *J. Geophys.*
609 *Res. Atmos.*, 118, 3956-3971, 2013.

610 Becker, T., Stevens, B., and Hohenegger, C. : Imprint of the convective
611 parameterization and sea surface temperature on large scale convective self-aggregation, *J.*
612 *Adv. Model Earth Syst.*, 9, 1488-1505, 2017.

613 Boberg, F., Berg, P., Thejll, P., Gutowski, W.J., and Christensen, J.H.: Improved
614 confidence in climate change projections of precipitation evaluated using daiy statistics from
615 the PRUDENCE ensemble, *Clim. Dyn.*, 32, 1097-1106, 2009.

616 Chen, C.T., and Knutson, T.: On the verification and comparison of extreme rainfall
617 indices from climate models, *J. Climate*, 21, 1605-1621, 2008.



618 Chou, C., Chen, C.-A., Tan P.-H., and Chen, K.T.: Mechanisms for global warming
619 impacts on precipitation frequency and intensity, *J. Clim.*, 25, 3291-3306, 2012.

620 Christensen, J.H., and Christensen, O.B.: Climate modeling: Severe summertime
621 flooding in Europe, *Nature*, 421, 805-806, 2003.

622 Easterling, D.R., Meehl, G.A., Parmesan, C., Changnon, S.A., and Mearns, L.O.:
623 Climate extremes: Observations, modeling and impacts, *Science*, 289, 2068-2074, 2000.

624 Fischer, E.M., and Knutti, R.: Observed heavy precipitation increase confirms theory
625 and early models, *Nature Climate Change*, 6, 986-990, 2016.

626 Flato, G., Marotzke, J., Abiodun, B., Braconot, P., Chou, S.C., Collins, W., Cox, P.,
627 Driouech, F., Emori, S., Eyring, V., Forest, C., Glecker, P., Guiliard, E., Jacob, C., Kattsov,
628 V., Reason, C., and Rummukainen, M.: Evaluation of climate models. Chapter 9 of *Climate
629 Change 2013. The Physical Science Basis. Contribution of Working Group I to the Fifth
630 Assessment Report of the Intergovernmental Panel on Climate Change*, Stocker T.F., et al.,
631 Eds., Cambridge University Press, Cambridge, United Kingdom and New York, NY, USA,
632 pp. 741-866, 2013.

633 Gao, X.J., Pal, J.S., and Giorgi, F.: Projected changes in mean and extreme
634 precipitation over the Mediterranean region from high resolution double nested RCM
635 simulations, *Geophys. Res. Lett.*, 33, L03706, 2006.

636 Giorgi, F., and Bi, X.: Regional changes in surface climate interannual variability for
637 the 21st century from ensembles of global model simulations, *Geophys. Res. Lett.*, 32,
638 L13701, 2005.

639 Giorgi, F., and Coppola, E.: Projections of 21st century climate over Europe, *European
640 Physical Journal, Web of Conferences*, 1, 29-46, 2009.



641 Giorgi, F., Shields Brodeur, C., and Bates G.T.: Regional climate change scenarios
642 over the United States produced with a nested regional climate model, *J. Climate*, 7, 375-399,
643 1994.

644 Giorgi, F., Jones, C., and Asrar, G.: Addressing climate information needs at the
645 regional level: The CORDEX framework, *WMO Bulletin*, 58, 175-183, 2009.

646 Giorgi, F., Im, E.-S., Coppola, E., Diffenbaugh, N.S., Gao, X.J., Mariotti, L., and Shi,
647 Y.: Higher hydroclimatic intensity with global warming, *J. Climate*, 24, 5309-5324, 2011.

648 Giorgi, F., Coppola, E., Solmon, F., Mariotti, L., Sylla, M.B., Bi, X., Elguindi, N.,
649 Diro, G.T., Nair, V., Giuliani, G., Turuncoglu, U.U., Cozzini, S., Guttler, I., O'Brien, T.A.,
650 Tawfik, A.B., Shalaby, A., Zakey, A.S., Steiner, A.L., Stordal, F., Sloan, L.C., and Brankovic,
651 C.: RegCM4: Model description and preliminary tests over multiple CORDEX domains,
652 *Clim. Res.*, 52, 7-29, 2012.

653 Giorgi, F., Coppola, E., Raffaele, F., Diro, G.T., Fuentes-Franco, R., Giuliani, G.,
654 Mangain, A., Llopart-Pereira, M., Mariotti, L., and Torma, C.: Changes in extremes and
655 hydroclimatic regimes in the CREMA ensemble projections, *Climatic Change*, 125, 39-51,
656 2014a.

657 Giorgi, F., Coppola, E., and Raffaele, F.: A consistent picture of the hydroclimatic
658 response to global warming from multiple indices: Modeling and observations, *J. Geophys.*
659 *Res.*, 119, 11,695-11,708, 2014b.

660 Giorgi, F., Torma, C., Coppola, E., Ban, N., Schar, C., and Somot, S.: Enhanced
661 summer convective rainfall at Alpine high elevations in response to climate warming, *Nature*
662 *Geoscience*, 9, 584-589, 2016.



663 Giorgi, F., Coppola, E., and Raffaele, F.: Threatening levels of cumulative stress due
664 to hydroclimatic extremes in the 21st century. *NPJ Climate and Atmospheric Science*, 1, 18,
665 doi:10.1038/s41612-018-0028-6, 2018.

666 Gutowski, W.J. Jr., Takle, E.S., Kozak, K.A., Patton, J.C., Arritt, R.W., and
667 Christensen, J.C.: A possible constraint on regional precipitation intensity changes under
668 global warming, *J. Hydrometeorol.*, 8, 1382-1396, 2007.

669 Gutowski, W.J. Jr, Giorgi, F., Timbal, B., Frigon, A., Jacob, D., Kang, H.-S.,
670 Krishnan, R., Lee, B., Lennard, C., Nikulin, G., O'Rourke, E., Rixen, M., Solman, S.,
671 Stephenson, T., and Tangang, F.: WCRP Coordinated Regional climate Downscaling
672 Experiment (CORDEX): A diagnostic MIP for CMIP6 Geoscientific Model Development, 9,
673 4087-4095, 2016.

674 Intergovernmental Panel on Climate Change (IPCC). Managing the risks of extreme
675 events and disasters to advance climate change adaptation, IPCC Special Report, Field C.B.,
676 et al., Eds., Cambridge University Press, Cambridge, U.K., 582 pp, 2012.

677 Intergovernmental Panel on Climate Change (IPCC). Climate Change 2013. The
678 Physical Science Basis. Contribution of Working Group I to the Fifth Assessment Report of
679 the Intergovernmental Panel on Climate Change, Stocker T.F., et al., Eds., Cambridge
680 University Press, Cambridge, United Kingdom and New York, NY, USA, 1029 pp, 2013.

681 Held, I.M., and Soden, B.J.; Robust responses of the hydrological cycle to global
682 warming, *J. Climate*, 19, 5686-5699, 2006.

683 Herold, N., Behrangi, A., and Alexander, L.V.: Large uncertainties in observed daily
684 precipitation extremes over land, *J. Geophys. Res. Atmos.*, 122, 668-681, 2017.



685 Ivancic, T.J., and Shaw, S.B.: A U.S. based analysis of the ability of the Clausius-
686 Clapeyron relationship to explain changes in extreme rainfall with changing temperature, J.
687 Geophys. Res. Atmos., 121, 3066-3078, 2016.

688 Jacob, D., Petersen, J., Eggert, P., Alias, A., Christensen, O.B., Bouwer, L.M., Braun,
689 A., Colette, A., Deque, M., Georgievski, G., Georgopoulou, E., Gobiet, A., Menut, L.,
690 Nikulin, G., Haensler, A., Hampelmann, N., Jones, C., Keuler, K., Kovats, S., Kroner, N.,
691 Kotlarski, S., Kriegsmann, A., Martin, E., van Meijgaard, E., Moseley, C., Pfeifer, S.,
692 Preuschmann, S., Radermacher, C., Radtke, K., Rechid, D., Rounsevell, M., Samuelsson, P.,
693 Somot, S., Soussana, J.F., Teichmann, C., Valentini, R., Vautard, R., Weber, B., and Yiou, P.:
694 EURO-CORDEX: New high resolution climate change projections for European impact
695 research, Regional Environmental Change, 14, 563-578, 2014.

696 Jones, C., Giorgi, F., and Asrar, G.: The COordinated Regional Downscaling
697 EXperiment: CORDEX. An international downscaling link to CMIP5, CLIVAR Exchanges,
698 16, 34-40, 2011.

699 Kharin, V.V., Zwiers, F.W., and Zhang, X.: Intercomparison of near surface
700 temperature and precipitation extremes in AMIP-2 simulations, reanalyses and observations,
701 J. Climate, 18, 5201-5233, 2005.

702 Lenderink, G., and van Meijgaard, K.: Increase in hourly extreme precipitation beyond
703 expectations from temperature change, Nature Geoscience, 1, 511-514, 2008.

704 Moss, R.H., Edmonds, J.A., Hibbard, K.A., Manning, M.R., Rose, S.K., van Vuuren,
705 D.P., Carter, P.R., Emori, S., Kainuma, M., Kram, T., Meehl, G.A., Mitchell, J.F.B.,
706 Nakicenovic, N., Rihai, K., Smith, S.J., Stouffer, R.J., Thompson, A.M., Weyant, J.P., and
707 Willbanks, T.J.: The next generation of scenarios for climate change research and assessment,
708 Nature, 463, 747-756, 2010.



- 709 Mueller, C.J., and Held, I.M.: Detailed investigation of the self-aggregation of
710 convection in cloud-resolving simulations. *J. Atm Sci.*, 69, 2551-2565, 2012.
- 711 Pall, P., Allen, M.R., and Stone, D.A.: Testing the Clausius-Clapeyron constraint on
712 changes in extreme precipitation under CO₂ warming, *Clim. Dyn.*, 28, 351-363, 2007.
- 713 Prein, A.F., Langhans, W., Fosser, G., Ferrone, A., Ban, N., Goergen, K., Keller, M.,
714 Tolle, M., Gutjahr, O., Feser, F., Brisson, E., Koller, S., Schmidli, J., van Lipzig, N.P.M.,
715 Leung, R.: A review on regional convection-permitting climate modeling: Demonstrations,
716 prospects and challenges, *Rev. Geophys.*, 53, 323-361, 2015.
- 717 Raisanen, J.: CO₂ - induced changes in interannual temperature and precipitation
718 variability in 19 CMIP2 experiments, *J. Climate*, 15, 2395-2411, 2002.
- 719 Rihai, K., van Vuuren, D.P., Kriegler, E., Edmonds, J., O'Neill, B.C., Fujimori, S.,
720 Bauer, N., Calvin, K., Dellink, R., Fricko, O., Luta, W., Popp, A., Cuaresma, J.C., Samir,
721 K.C., Leimbach, M., Jiang, L., Kram, T., and Rao, S.: The Shared Socioeconomic Pathways
722 and their energy, land use, and greenhouse gas emissions implications: An Overview, *Global*
723 *Environmental Change*, 42, 153-168, 2016.
- 724 Ruti, P., Somot, S., Giorgi, F., Dubois, C., Flaounas, E., Obermann, A., Dell'Aquila,
725 A., Pisacane, A., Harzallah, A., Lombardi, E., Ahrens, B., Akhtar, N., Alias, A., Arsouze, T.,
726 Aznar, R., Bastin, S., Bartholy, J., Beranger, K., Beuvier, J., Bouffies-Cloche, S., Brauch, J.,
727 Cabos, W., Calmanti, S., Calvet, J.C., Carillo, A., Conte, D., Coppola, E., Djurdjevic, V.,
728 Drobinski, P., Elizalde, A., Gaertner, M., Galan, P., Gallardo, C., Goncalves, M., Gualdi, S.,
729 Jorba, O., Jorda, G., Lheveder, B., Lebeaupin-Brossier, C., Li, L., Liguori, G., Lionello, P.,
730 Macias-Moy, D., Nabat, P., Onol, B., Rajkovic, B., Ramage, K., Sevault, F., Sannino, G.,
731 Struglia, M.V., Sanna, A., Torma, G., and Vervatis, V.: MED-CORDEX initiative for
732 Mediterranean climate studies, *Bull. Am. Met. Soc.*, 97, 1187-1208, 2016.



733 Schiemann, R., Demory, M.-E., Shaffrey, L.C., Strachan, J., Vidale, P.L., Mizielinski,
734 M.S., Roberts, M.J., Matsueda, M., Wehner, M.F., and Jung, T.: The resolution sensitivity of
735 northern hemisphere blocking in 4 25-km atmospheric global circulation models, *J. Climate*,
736 30, 337-358, 2017.

737 Sillmann, J., Kharin, V.V., Zwiers, F.V., Zhang, X., and Bronaugh, D.: Climate
738 extreme indices in the CMIP5 multimodel ensemble: Part 2. Future climate projections, *J.*
739 *Geophys. Res.*, 118, 2473-2493, 2013a.

740 Sillmann, J., Kharin, V.V., Zhang, X., Zwiers, F.W., and Bronaugh, D.: Climate
741 extreme indices in the CMIP5 multimodel ensemble. Part I: Model evaluation in the present
742 climate, *J. Geophys. Res.*, 118, 1716-1733, 2013b.

743 Taylor, K.E., Stouffer, R.J., and Meehl, G.A.: An Overview of CMIP5 and the
744 Experiment Design, *Bull. Amer. Meteor. Soc.*, 93, 485-498, 2012.

745 Tebaldi, C., Hayhoe, K., Arblaster, J.M., and Meehl, G.A.: Going to the extremes: An
746 intercomparison of model-simulated historical and future changes in extreme events, *Climatic*
747 *Change*, 79, 185-211, 2006.

748 Trenberth, K.E.: Conceptual framework for changes of extremes of the hydrological
749 cycle with climate change, *Clim. Change*, 42, 327-339, 1999.

750 Trenberth, K.E.: Changes in precipitation with climate change, *Clim. Res.* 47, 123-
751 138, 2011.

752 Trenberth, K.E., Dai, A., Rasmussen, R.M., and Parsons, D.B.: The changing
753 character of precipitation, *Bull. Am. Meteor. Soc.*, 84, 1205-1217, 2003.



754 Trenberth, K.E., Smith, L., Qian, T., Dai, A., and Fasullo, J.: Estimates of the global
755 water budget and its annual cycle using observational and model data, *J. Hydrometeorology*,
756 8, 758-769, 2007.

757 Warner, T.T.: *Numerical Weather and Climate Prediction*, Cambridge University
758 Press, Cambridge U.K., 526 pp., 2010.

759 Wehner, M.F., Smith, R.L., Bala, G., and Duffy, P.: The effect of horizontal resolution
760 on simulation of very extreme US precipitation events in a global atmosphere model, *Clim.*
761 *Dyn.*, 24, 241-247, 2010.